Experimental Fluid Mechanics of Pulsatile Artificial Blood Pumps

Steven Deutsch,[1] John M. Tarbell,[2] Keefe B. Manning,[1] Gerson Rosenberg,[1,3] and Arnold A. Fontaine[1]

[1]Department of Bioengineering, Pennsylvania State University, University Park, Pennsylvania 16802; email: sd1@wt.arl.psu.edu, kbm10@psu.edu, aaf@wt.arl.psu.edu

[2]Department of Biomedical Engineering, City College of New York, New York, New York 10031; email: tarbell@ccny.cuny.edu

[3]Divison of Artificial Organs, Department of Surgery, Pennsylvania State Milton S. Hershey Medical Center, Hershey, Pennsylvania 17033; email: grosenberg@psu.edu

Annu. Rev. Fluid Mech.
2006. 38:65–86

The *Annual Review of Fluid Mechanics* is online at fluid.annualreviews.org

doi: 10.1146/annurev.fluid.38.050304.092022

0066-4189/06/0115-0065$20.00

Key Words

artificial heart, pusatile blood pumps, hemolysis, thrombosis, wall shear stress, particle image velocimetry

Abstract

The fluid mechanics of artificial blood pumps has been studied since the early 1970s in an attempt to understand and mitigate hemolysis and thrombus formation by the device. Pulsatile pumps are characterized by inlet jets that set up a rotational "washing" pattern during filling. Strong regurgitant jets through the closed artificial heart valves have Reynolds stresses on the order of 10,000 dynes/cm^2 and are the most likely cause of red blood cell damage and platelet activation. Although the flow in the pump chamber appears benign, low wall shear stresses throughout the pump cycle can lead to thrombus formation at the wall of the smaller pumps (10–50 cc). The local fluid mechanics is critical. There is a need to rapidly measure or calculate the wall shear stress throughout the device so that the results may be easily incorporated into the design process.

INTRODUCTION

Although the use of mechanical circulatory support was postulated as early as 1812 by LeGallois (LeGallois et al. 1813), it was not until 1961 that the first clinical left heart bypass was performed by Hall et al. (1962). It was almost eight years later that Cooley (1969) implanted the first artificial heart into the chest of a patient for over 60 hours before replacing the device with a human donor heart. Although the promise of clinically acceptable devices with widespread use was predicted by many researchers, progress was slower than anticipated due to difficulties with bleeding, hemolysis, thrombus formation, infection, and device failure. Thrombus formation and hemolysis appeared to be fundamental problems limiting device success. In spite of the use of anticoagulant and platelet-inhibiting agents, thrombus formation and embolic events were common. Under certain operating conditions, hemolysis was also encountered. It was recognized that thrombus formation and hemolysis within blood pumps was influenced by several factors such as the blood material interface, the surface topography, and the fluid mechanics.

Researchers realized flow visualization could be implemented in the design of blood pumps to reduce thrombus formation, which is influenced by fluid mechanics. In 1971, Phillips et al. (1972) performed pioneering studies utilizing flow visualization techniques in blood pumps. Results of these studies indicated that changes in blood pump geometry, valve type, and orientation could reduce thrombus formation. For example, a region of stasis that existed in the apex of the blood pump was eliminated by replacing a ball and cage valve with a tilting disc valve.

Measurement techniques for studying blood flow in artificial hearts were pioneered in the Pennsylvania State University Artificial Heart research lab. Early studies used particle tracers such as pearl essence. A heated wire producing hydrogen bubbles was also used in the entrance region of the pump. Techniques such as hot film anemometry, laser Doppler anemometry (LDA), and, more recently, particle image velocimetry (PIV), have all been employed to study details of the flow field within blood pumps and have resulted in significant improvements in blood pump design.

GENERAL DESCRIPTION

Pulsatile Artificial Hearts and Ventricular Assist Devices

The LionHeart^{TM} Left Ventricular Assist System, shown in **Figure 1**, illustrates one end product of experimentation discussed here. In the pulsatile pumps, the flow is driven either pneumatically or by a pusher plate against a segmented polyurethane blood sac. Where measurement access to the ventricle is required, the blood sac is replaced by a diaphragm of the same material, so that the interior of the model is exposed. This is a good representation of pusher plate devices, where only the pusher plate side of the sac moves. Generally, the device is cylindrical, with ports for the inlet and outlet artificial heart valves that are joined tangentially to the body. For an adult device under physiologic conditions, the mean aortic (outlet) pressure is 100 mm Hg (120/80), the mean atrial (inlet) pressure is 10mm Hg (20/0), and the

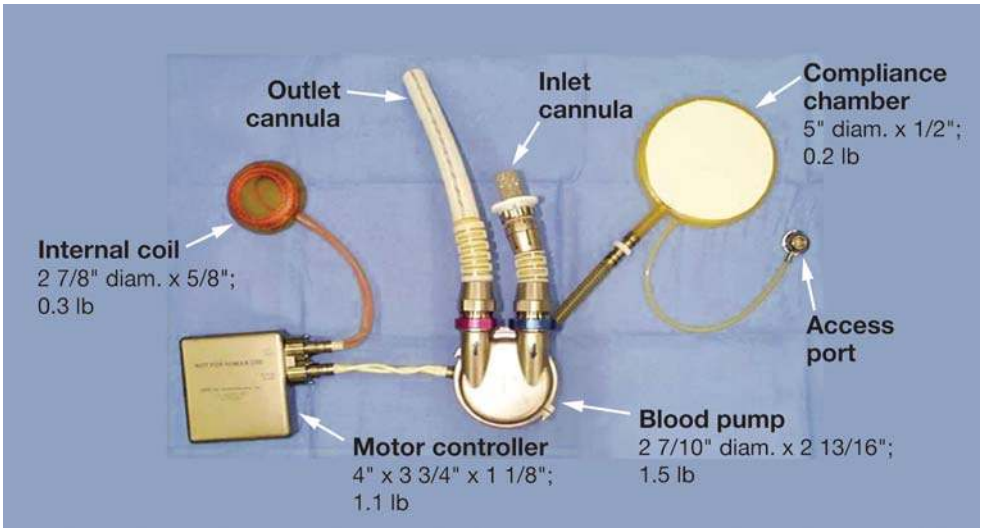

Figure 1

The LionHeart^{TM} Left Ventricular Assist System.

cardiac output is 5 liters/min. The beat rate is 72 beats/min (bpm) and the percentage of the cycle in outlet flow (systolic duration) is 30% to 50%. Physiological conditions can vary widely and automatic control of the pump cycle is normally through monitoring of the end diastolic volume, diastole being the filling portion of the cycle. Mehta et al. (2001) provides a description of a typical, fully implantable device. Much of the characterization of the fluid mechanics of pulsatile, artificial blood pumps has been by our group at Penn State, so this review necessarily focuses on those results.

The Mock Circulation

Rosenberg et al. (1981) describe a mock circulatory loop for testing the blood pumps. Inlet and outlet compliance chambers simulate the atrial and aortic compliance of the native cardiovascular system, while a parallel plate resistor downstream of the aortic compliance simulates the systemic resistance of the circulation. A reservoir between the systemic resistance and atrial compliance controls the preload to the pump. Pressure waveforms are measured in the compliance chambers and flow waveforms at the inlet and outlet ports. The variable compliance and resistance are used to set the fixed flow conditions. Beat rate and systolic duration are also parameters and are set through an appropriate drive system. The dynamic control of the implanted device has not been simulated but is described by Mehta et al. (2001).

Blood Analog Fluids

Blood is a shear thinning, viscoelastic fluid (Cokelet 1987) that is often taken as Newtonian at sufficiently high shear rates (above 500 s^{-1}). The hematocrit (relative

volume of red blood cells) greatly affects the magnitude and relative importance of the viscous and elastic components of the complex viscosity (Thurston 1996). The high shear rate kinematic viscosity asymptote for normal hematocrit blood (40%) is about 3.5 centistokes (cs) and solutions of glycerin and water (40/60) or mineral oils are often taken as blood analogs (Hochareon et al. 2003). Optical access to the fluid for velocity measurements can be important and Baldwin et al. (1994), among others, used a solution of 79% saturated aqueous sodium iodide, 20% pure glycerol, and 1% water by volume to produce a fluid with a kinematic viscosity of 3.8 cs and an index of refraction (matching Plexiglas) of 1.49 at 25°C. Using a Newtonian analog is often justified on the grounds that blood hemolysis is a result of strong shear flows and turbulence, which are characterized by high shear rates. Mann et al. (1987) compared Newtonian and viscoelastic solutions against bovine blood in an artificial ventricle using ultrasound and found that the viscoelastic material tracked the bovine blood better. Brookshier & Tarbell (1993) developed Xanthan gum/glycerin solutions that simulate blood viscoelasticity well; sodium iodide may be added to adjust the index of refraction.

Heart Valves

Heart valves, which maintain unidirectional flow, play a major role in the mechanical environment of the artificial heart. They are generally chosen for their durability. For the Penn State devices, Bjork-Shiley tilting disc valves were used. For a 70-cc pump, the outlet valve port is 27 mm and the inlet port is 29 mm. Mechanical heart valves (MHVs) are not specifically designed for mechanical blood pump flow fields, and their efficiency can be compromised. Yoganathan et al. (2004) gives a survey of MHVs and their fluid mechanics. Some discussion of the effect of MHVs in the artificial heart or blood pump environment follows in context with different-size devices.

Hemolysis and Thrombosis

Hemolysis, the destruction of red blood cells, and thrombosis, clot formation, must be avoided in artificial blood pumps to achieve long-term clinical success. The relationship of these events to the fluid mechanics, velocity, shear and wall shear rates, and turbulence is the major impetus for flow studies in blood pumps. Neither phenomenon is completely understood. A hemolysis potential curve from the National Heart, Lung, and Blood Institute (1985), which relates shear stress and exposure time to red cell, white cell, and platelet lysis has been available since 1985. Because blood cells are viscoelastic, they can tolerate high stresses for short exposure times without hemolysis. For example, an exposure time of more than 0.1 ms at a shear stress of 10,000 dynes/cm^2 will produce red cell lysis as will 1500 dynes/cm^2 for times over 100 s. Nevaril et al. (1969) concluded that prolonged exposure to laminar shear stress on the order of 1500 dynes/cm^2 could cause lysis of red cells, and Sallam & Hwang (1984) showed that sustained turbulent stresses above 4000 dynes/cm^2 created by a submerged jet would cause hemolysis. Baldwin et al. (1994) concluded, on the basis of these and other published studies, that stress levels above 1500–4000 dynes/cm^2

were undesirable. Platelet activation and the initiation of the clotting process may occur at still lower stresses.

Thrombus formation has long been thought to be a function of, among other factors, (low) wall shear stress and blood residence time (see Wootton & Ku 1999 for example). Hubbell & McIntire (1986) reported that the wall shear rate should be above 500 s^{-1} [18 dynes/cm^2 for a viscosity of 3.5 centipoise (cp)] to prevent clot formation on segmented polyurethane (the blood sac material). Daily et al. (1996) pointed out that "the thrombogenicity of assist devices can be attributed to (1) the coagulability of the blood, (2) the properties of the blood contacting surfaces, and (3) fluid dynamic factors." It is often not easy to separate these.

EARLY EXPERIMENTS IN BRIEF

Early fluid mechanics studies were through flow visualization (Lenker 1978, Phillips et al. 1972), single-component laser Doppler anemometry (Phillips et al. 1979), hot film anemometry in conjunction with dye washout (Affeld 1979), and pulsed Doppler ultrasound (Mann et al. 1987, Tarbell et al. 1986). Flow visualization continues to be useful for qualitative assessment. More recent flow visualization studies are by Hochareon et al. (2003), Mussivand et al. (1988), and Woodward et al. (1992), for example.

Mann et al. (1987) used pulsed Doppler ultrasound to measure the near wall flow at 13 locations around the cylindrical portion of a 100-cc artificial heart model using glycerin/water, bovine blood, and a 0.08% by weight separan (a shear thinning polymer) solution. They estimated their control volume, which was angled at 60° to the wall, as a cylinder of 3 mm in diameter and a thickness of 0.45 mm. In addition, because only a single component of velocity was measured, assumptions about the flow field had to be made for wall shear rates to be estimated. Flow patterns for the three test fluids were quite different, particularly during diastole, where it was speculated that the viscoelasticity of the separan solution and the bovine blood reduced the spread of the inlet jet. Tarbell et al. (1986), using the same system under the same assumptions, found peak wall shear stresses of less than 30 dynes/cm^2. They concluded that the mean and turbulent flow in the ventricular assist device (VAD) was not high enough to damage blood elements, but that the low wall shear could contribute to thrombus deposition. The pulsed Doppler ultrasound measurements suffered from poor spatial resolution.

In an important study, Jarvis et al. (1991) used human blood in a 100-cc artificial ventricle to measure hemolysis directly through quantification of plasma-free hemoglobin. They found that the degree of hemolysis was a function of the operating conditions of the ventricle. For example, 90 bpm produced a third more hemolysis than did 60 bpm, with both at 50% systolic duration. The authors speculated that the turbulent stresses might play an important role.

Baldwin et al. (1988) did extensive measurements of wall shear stress inside a ventricle using flush-mounted hot film anemometry probes. The artificial ventricle was large (100 cc) and had an inlet port at the center of the device—a configuration no longer used. This makes it difficult to compare their results with those of other

investigators in smaller pumps. The pump was run at physiologic conditions. Peak wall shear stresses were in the range of 350–500 dynes/cm^2 in the body of the device, essentially independent of systolic duration. There was no evidence of flow stagnation. Near the valves, values of the wall shear stress were of the order 1000–1500 dynes/cm^2 at 50% systolic duration and nearly twice that for 30% systolic duration. The authors concluded that flow in the body of the device was probably not hemolytic while the shear stress levels in the valve passages were. Francischelli et al. (1991) used a fiber optic system to look at residence times for an analog fluid doped with fluorescein dye. Both a 70-cc parallel port device (Baldwin et al. 1994) and the 100-cc device considered by Baldwin et al. (1988) were studied at systolic durations of 30% and 50%. They found that the washout is characterized by an exponential decay. For all positions and operating conditions considered, washout was within 1–2 beats.

A 70-CC ADULT DEVICE

Baldwin et al. (1989, 1990, 1993, 1994) published what is still the most thorough study of artificial heart fluid mechanics. They used a two-component laser Doppler anemometer to make mean and turbulence measurements at some 135 locations within the ventricle and 10 locations at each of the outlet and inlet flow tracts at normal physiologic conditions. A standard four-beam, two-component system was used in backscatter, with counter signal processors, to perform the measurements. The measurement ellipsoids had a diameter of roughly 65 μm and a length of 1.13 mm. The beat cycle was divided into eight time windows, centered about 0, 100, 200, 300, 400, 500, 600, and 700 ms after the start of systole. Time windows varied from 20 to 100 ms, as a function of data rate (as described by Baldwin et al. 1993), with 40 ms used for most cycle times and locations. Coincident data occurring during any time of interest was placed in the appropriate time window file. Mean and fluctuating velocities and Reynolds stresses were calculated from 250 ensembles at each time window and location. Baldwin et al. (1993) estimated that 95% of the Reynolds stresses would be within 20% of the (converged) values obtained for 4096 ensembles.

The Reynolds stresses are not invariant to coordinate rotations, so that data was presented, in principle axes, as the maximum Reynolds normal and shear stress (Baldwin et al. 1993). A problem inherent to turbulence measurements of this nature is that the beat-to-beat variation of the flow will appear as a "pseudo turbulence" that cannot be separated out. Setting a single "coincidence time" in these unsteady flows may also lead to errors in the stress. In addition, we note, as do the authors, that it is not clear how the Reynolds stresses are related to the damage of red blood cells—roughly 3 × 8-μm, biconcave disks. Perhaps the case can be made, as the authors do, that the turbulent dissipation will increase as the Reynolds stress to the 3/2, so that the Kolmogorov scale, proportional to the stress to the −3/8, will be smaller as the stress increases and therefore more dangerous to the red cells. Some estimates by Baldwin et al. (1994) suggest that the small-scale structure of regurgitant jets through the closed valves is the order of 5 μm, as discussed below.

We reproduce the mean velocity map of the chamber flow in **Figure 2**. Mean velocities in the chamber are not available at 300 and 400 ms into the cycle (during

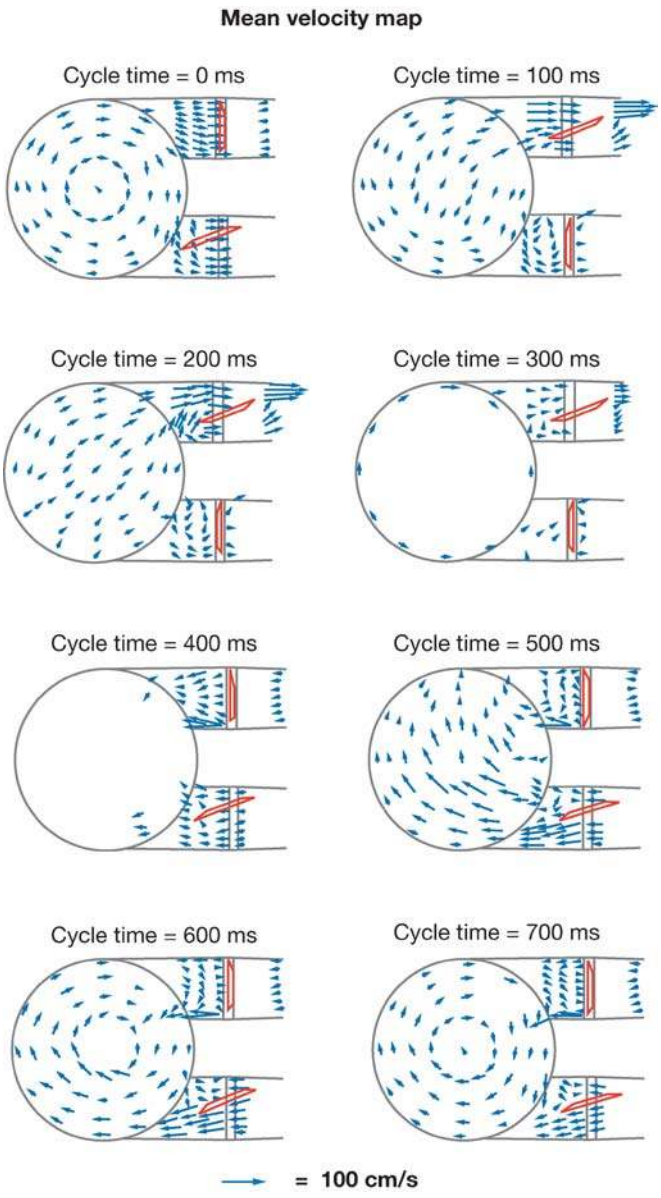

Figure 2

Mean (ensemble-averaged) velocity maps of a 70-cc device at eight times during the cardiac cycle. Time zero is the onset of systole, diastole begins at 400 ms, and the cycle duration is 800 ms. Arrow lengths are proportional to mean velocity magnitude (see scale) and point in the direction of the mean velocity vector. The aortic (ejecting) port is located at the top and the mitral (filling) port is located at the bottom. (Permission granted from ASME, Baldwin et al. 1994.)

systole), as the beams are blocked by the pusher plate. The highest velocities in the chamber are in the major orifices of the aortic valve [1.9 meters/second (m/s)] and of the mitral valve (1.2 m/s) in early systole and early diastole, respectively. The inlet jet through the major orifice helps to produce a rotational pattern in the chamber that persists into early systole (0–500 ms). The authors note that this rotational pattern appears to provide good "washing" of the chamber. Other experiments, with sac-type

artificial hearts, note quite similar flow patterns (see, for example, Jin & Clark 1993). However, Baldwin et al. (1994) demonstrate that the minor orifice of the mitral valve does not show significant inflow during diastole (400–700 ms), and that this may be a result of the rotational motion "clipping" the incoming flow. Of great interest are the large retrograde fluid velocities, through the "closed" valves, in the near wall regions of the aortic valve during diastole and the mitral valve during systole.

The major Reynolds normal stresses are shown in **Figure 3**. Major Reynolds shear stresses are half these values and are rotated 45° clockwise from the principle stress axis. The authors note that major normal stresses do not exceed 1000 dynes/cm^2 in the chamber and 2000 dynes/cm^2 in the aortic outflow tract. The outflow values are similar to those observed by Yoganathan et al. (1986) with this valve. Much larger Reynolds stresses were found in the regurgitant (retrograde) jets, prompting the authors to study these in more detail. The mitral valve regurgitant jet is stronger than that of the aortic valve because of the larger pressure gradient across it during systole than across the aortic valve during diastole. Velocities as high as 4.4 m/s and normal stresses as large as 20,000 dynes/cm^2 were observed.

Baldwin et al. (1994) conclude by asking whether "artificial heart fluid mechanics can be improved." They base this on the rather innocuous fluid mechanics of the pumping chamber and the relatively minor ways in which the geometry, with respect to the size and shape of the natural heart, may be changed. They find that the near valve flow is of concern. Maymir et al. (1997, 1998) continued the study of regurgitant jets, in particular, the influence of occluder to housing valve gap width. Meyer et al. (1997, 2001) extended the work by using a three-component LDA for three additional MHVs—the Medtronic-Hall tilting disc, and the Carbomedics and St. Jude bileaflet designs—and report turbulent jets with large sustained Reynolds stress even for the bileaflet valves.

An additional concern with using MHVs is the recognition (Leuer 1986, Quijano 1988, Walker 1974) that they cavitate. Cavitation is the formation of bubbles from gaseous nuclei in the fluid due to a drop in local pressure (Young 1989). Although Zapanta et al. (1996) showed valve cavitation in vivo in an artificial heart, the problem is not just associated with the use of MHV in the artificial heart, but with the general use of these valves. There are several serious potential problems associated with cavitation: hemolysis and thrombosis initiation, valve leaflet damage, and the formation of stable gas bubbles that may find their way to the cranial circulation. Although cavitation-induced pitting of explanted valves has been observed (Kafesian et al. 1994), significant valve leaflet damage is rare. Lamson et al. (1993) used porcine blood to determine the index of hemolysis for three phases of the prosthetic heart valve flow cycle—forward flow, rapid valve closure, and regurgitant flow through the closed valve. They found that the hemolytic effect of regurgitant flow is equivalent to that of forward flow, under conditions producing no cavitation, even though the volume of backflow is much smaller than that of forward flow. This supports the order of magnitude higher Reynolds stresses observed in regurgitant flow compared to forward flow described by Maymir et al. (1997, 1998). Moreover, Lamson et al. (1993) show that the index of hemolysis is a strong function of cavitation intensity and cavitation duration.

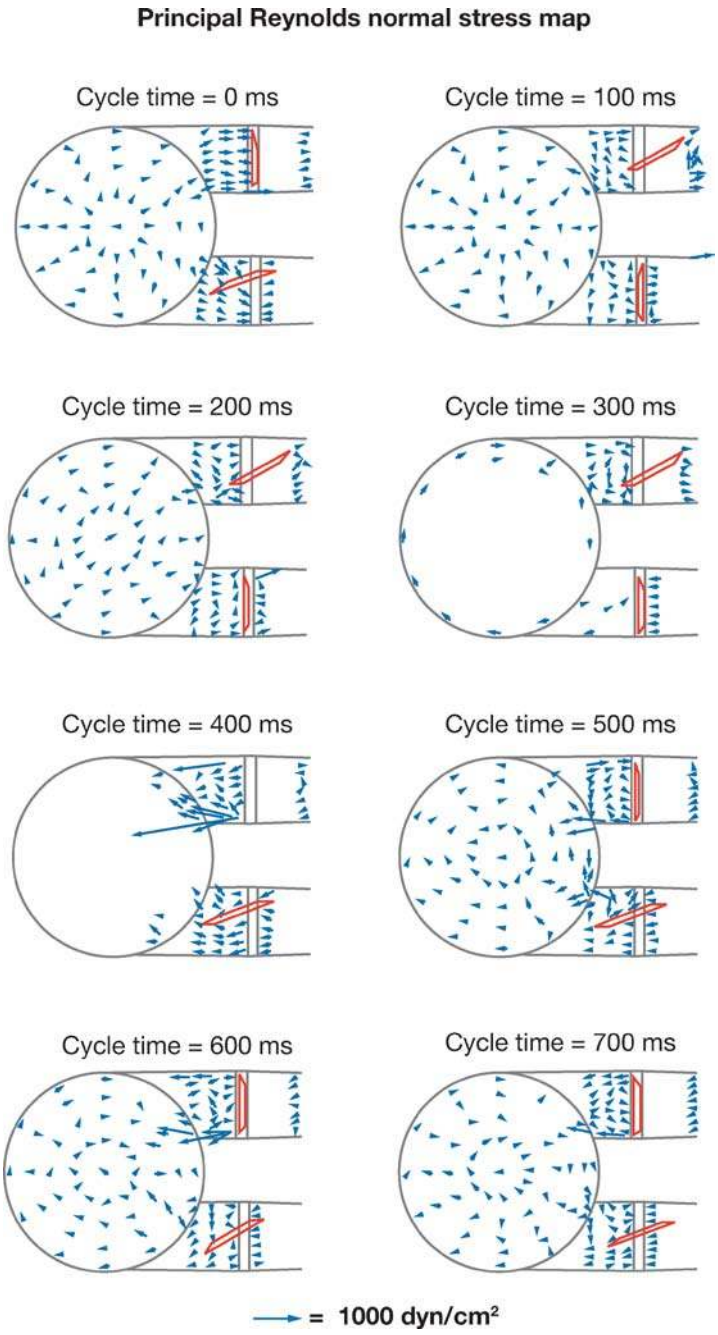

Figure 3

Major Reynolds normal stress maps of a 70-cc device at eight times during the cardiac cycle. Time zero is the onset of systole, diastole begins at 400 ms, and the cycle duration is 800 ms. Arrow lengths are proportional to normal stress magnitude (see scale) and point in the direction of the major axis of the principal stress axes. The aortic (ejecting) port is located at the top and the mitral (filling) port is located at the bottom. (Permission granted from ASME, Baldwin et al. 1994.)

There have been reports (for example, Dauzat et al. 1994) of gaseous emboli in the cranial circulation, detected by Doppler ultrasound, for MHV recipients. Bachmann et al. (2001), Biancucci et al. (1999), and Lin et al. (2000) suggest that these emboli might be the aftermath of cavitation growth and collapse. A good deal of work has been reported on MHV cavitation. There is no current review but much is described in the work of Graf et al. (1994), Zapanta et al. (1996), Chandran et al. (1997), and Bachmann et al. (2001).

SMALL BLOOD PUMPS

Pediatric Blood Pumps

The growing need for long-term pediatric, circulatory assist has resulted in a NIH program to develop such an assist device by 2009. The required output of the device is about 1 liter/min. The simple geometric scaling of the pumps is described by Bachmann et al. (2000). For example, to reduce the volume from 70 to 15 cc, one might reduce all linear dimensions by the cube root of the ratio of volumes. Assuming that the non-Newtonian nature of blood does not introduce any additional parameters, the "global" fluid dynamics of the system is described by the Reynolds (Re) and Strouhal (St) numbers. In a study of 73 healthy subjects ranging in age from 5 days to 84 years, Gharib et al. (1994) found that the Strouhal number remained fairly constant at 4–7. Later, Bachmann et al. (2000) assumed length, time, and velocity scales are, respectively, the diameter of the inlet port (di), half the inverse frequency (f) (for 50% systolic duration), and the mean volume flow rate divided by the area of the inlet port. With the volume flow rate equal to the stroke volume (SV) times frequency, they showed that $\mathrm{Re} = \left(\frac{8}{\pi\nu}\right)\frac{f \cdot SV}{d_i}$ and $St = \left(\frac{4}{\pi}\right)\frac{SV}{d_i^3}$. Clearly, geometrically similar pumps have constant Strouhal number.

Daily et al. (1996) and Bachmann et al. (2000) have both studied a roughly 15-cc pediatric assist device. Reynolds and Strouhal numbers for the devices, taken from Bachmann et al. (2000), are given in **Table 1**. The large increase in St for the 15-cc device is a result of undersizing the inlet port.

Table 1 Comparison of the Reynolds and Strouhal numbers for the 70-, 50-, and 15-cc artificial blood pumps*

Pump size	Reynolds	Strouhal
Penn State 70-cc device	2482	8.3
Penn State 50-cc device	1054	4.5
Penn State 15-cc device	1567	45.3
Yonsei 34-cc device	1500	7.7
Toyobo 20-cc device	988	6.3
MEDHOS-HIA 10-cc device	655	7.4
Berlin Heart 12-cc device	785	8.8

* Data adapted from tables 1 and 4 of Bachmann et al. 2000.

Daily et al. (1996) provided both PIV maps and clinical studies of the device that focused on the choice of MHVs—handmade ball and cage valves (which were initially used clinically) versus bileaflet valves. The PIV maps compared valve types for a single instant of diastole and a single instant of systole. They reported that for the bileaflet valve the inlet jet penetrated more deeply into the chamber and was more coherent; the diastolic rotational motion was formed sooner and the amount of fluid entrained by the outlet jet was greater. In addition, the pressure drop and mean energy loss through the ball and cage valves were much greater than that through the bileaflet. Moreover, they reported that animal experiments of the device with handmade ball and cage valves showed thrombus formation in the device—something rarely seen in the 70-cc pumps. Initial experiments with the bileaflet valves showed no such thrombus formation.

Bachmann et al. (2000) used a TSI Inc. two-component LDA system to measure mean and turbulence quantities in a pediatric ventricle with handmade ball and cage valves at normal physiologic conditions. By using beam expansion they reduced each measurement volume to a roughly 200 μm $\times$ 30 μm ellipse. At each of 75 locations, 250 ensembles were measured at distances from the wall opposite the pusher plate of 0.1, 0.3, 0.6, and 1.0 mm. The data reduction follows (Baldwin et al. 1994). Both a sodium iodide solution and a Xanthan gum viscoelastic solution were employed. The wall shear rate was estimated from the velocity measurement 0.1 mm from the wall, using the no-slip condition. A gray-scale contour map of the average wall shear stress over the filling portion of the cycle is shown for each fluid in **Figure 4** (the mitral port is located on the right side of the device). Large regions of very low wall shear stress are apparent. A similar plot for the wall shear stresses averaged over the ejection portion

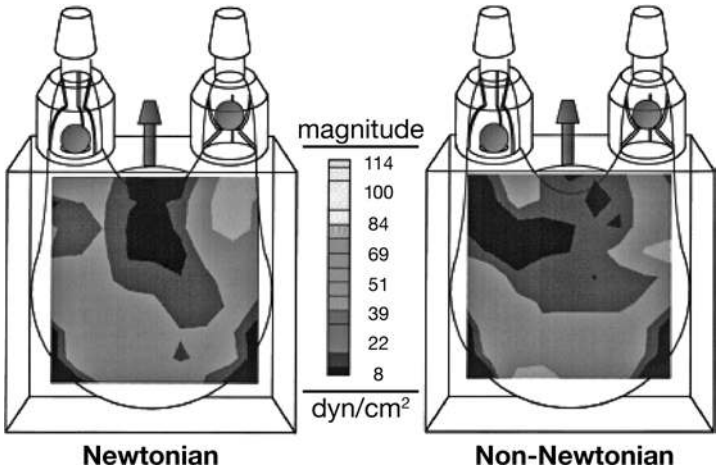

Figure 4

The diagrams of a pediatric device design show wall shear stresses averaged over the filling portion of the cardiac cycle for both Newtonian (*left*) and non-Newtonian fluids (*right*). (Permission granted by Blackwell Publishing, Bachmann et al. 2000)

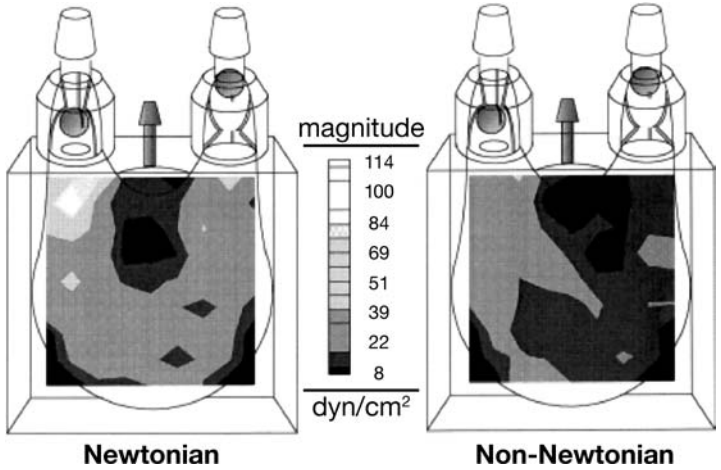

Figure 5

The diagrams of a pediatric device design show wall shear stresses averaged over the ejection portion of the cardiac cycle for both Newtonian (*left*) and non-Newtonian fluids (*right*). (Permission granted by Blackwell Publishing, Bachmann et al. 2000.)

of the cycle is shown in **Figure 5**. Again, we observe large regions of very low shear stresses. Differences between the results for each fluid, particularly on the inlet side of the model, are striking. Bachmann et al. (2000) compare the characteristics of the Penn State pediatric pump with other small pumps that have shown some clinical promise. These include pumps described by Park & Kim (1998), who use Carbomedics bileaflet valves; by Taenaka et al. (1990) and Takano et al. (1996), who use Bjork-Shiley tilting disk valves; and by Konertz et al. (1997a,b), who use polyurethane trileaflet valves. A consequence of using commercially available valves is a larger inlet length scale and reduced Strouhal number. Comparisons among the pumps, adapted from Bachmann et al. (2000), are shown in **Table 1**.

A 50-cc Device

The 70-cc–100-cc ventricles described earlier are too large, as the basis for implantable artificial hearts and blood pumps, to be used for much of the adult population. The development of smaller blood pumps that do not sacrifice cardiac output is a continuing research area. Hochareon et al. (2003, 2004a,b,c) and Oley et al. (2005) recently presented a study of the mean velocity and wall shear stress in a 50-cc device using high-speed video and PIV.

Hochareon et al. (2003) examined the opening pattern of the diaphragm using high-speed video. They determined that the opening pattern of the diaphragm, as it affected the diastolic jet and subsequent rotational motion, was a critical aspect of the overall flow. By comparison against flow visualization of the sac motion in a clinically approved 70-cc device, they also showed that the diaphragm motion was a good representative of the whole sac motion. Jin & Clark (1994) reported a similar study.

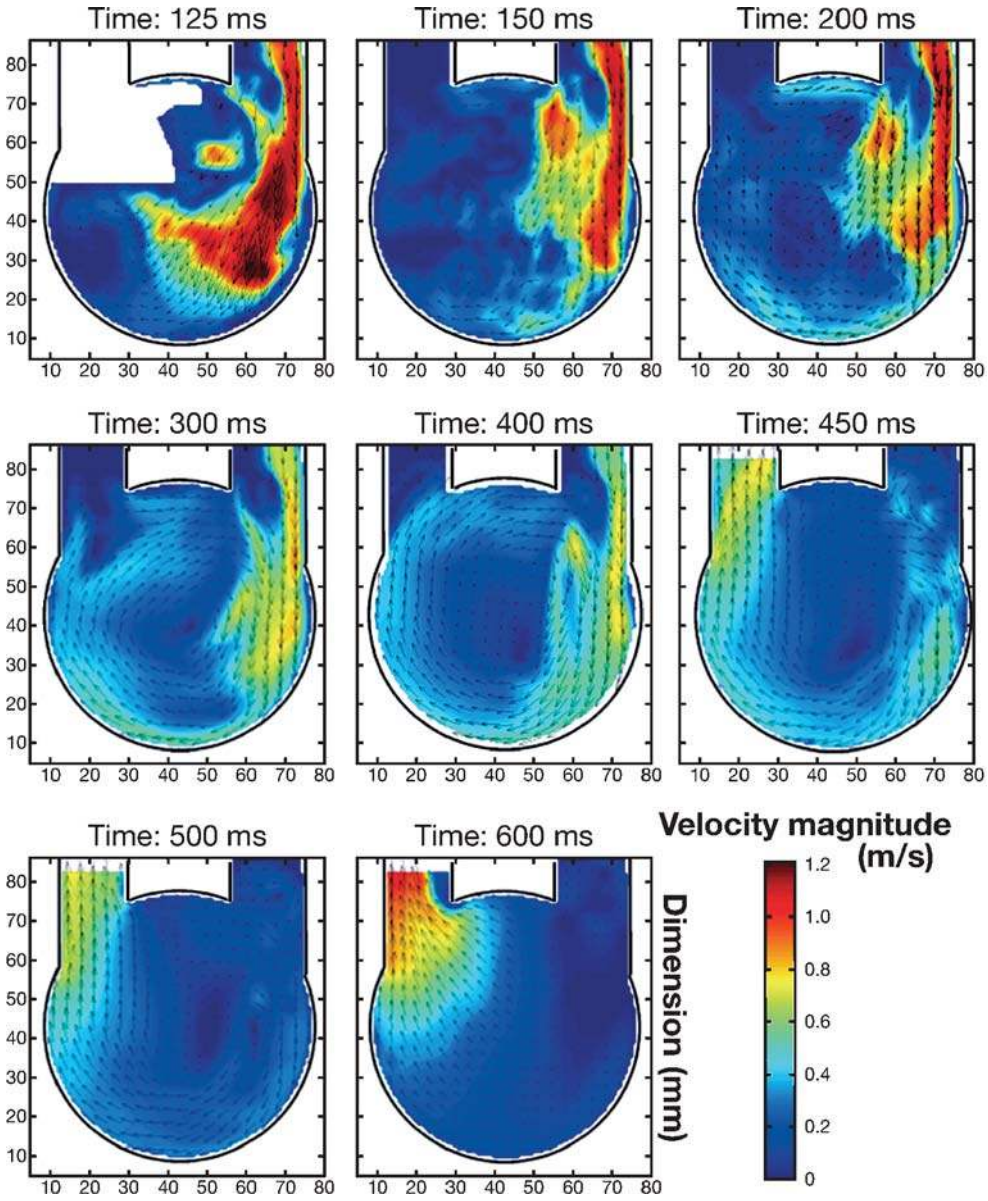

Figure 6

The particle image velocimetry (PIV) velocity maps during early diastole (125 and 150 ms), middle to late diastole (200–400 ms), and systole (450–600 ms) for the 50-cc Penn State ventricular assist device. Time reference is from the onset of diastole.) (Permission granted from ASME, Hochareon et al. 2004.)

Hochareon et al. (2004a,b,c) made PIV measurements in the transparent 50-cc pump model as a function of pump cycle time. The Reynolds and Strouhal number are included in **Table 1**. All measurements were in the plane of the pusher plate. In this design, however, the inlet valve is rotated 30° from the pusher plate direction, so that the light sheet is not aligned with the maximum jet velocity. The blood analog fluid was mineral oil. The pump was run at physiological conditions. A standard, planar TSI, Inc. PIV system was used to acquire 200 images at each condition. The light sheet was estimated at less than 0.5-mm thick and was initially centered 5 mm from the front edge. Cross-correlation of the images was performed by the TSI, Inc., Insight^{TM} software. The final interrogation window size was 16 × 16 pixels. Both a global and eight local areas (medial and lateral walls of the mitral and aortic ports and walls of the chamber body) were investigated. Resolution was 85 μm/pixel and 25 μm/pixel for the global and local maps, respectively. Components of the velocity gradient were calculated as central differences and wall shear rates estimated from the velocity point nearest the wall. The authors did not attempt to use PIV to estimate the turbulence levels.

Global flow maps are shown in **Figure 6**. Note that diastole starts at 0 ms and systole at 430 ms with the mitral port on the right side of the chamber. The flow is again dominated by the diastolic jet and subsequent large-scale rotation. Peak velocities are the order of those observed by Baldwin et al. (1994) in a 70-cc device. The authors use vorticity maps to highlight the growth of the wall boundary layers. The local flow field near the mitral port at 200 and 400 ms is reproduced in **Figure 7**. The associated wall shear rates shown in **Figure 8** never exceed some

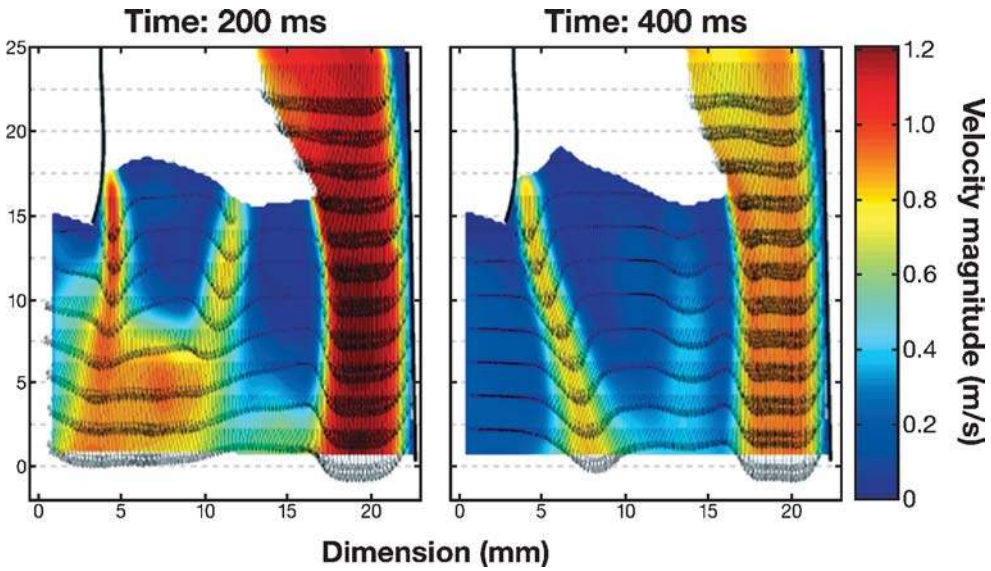

Figure 7

The velocity maps of the mitral port at 200 ms and 400 ms for the 50-cc Penn State ventricular assist device. (Permission granted from ASME, Hochareon et al. 2004.)

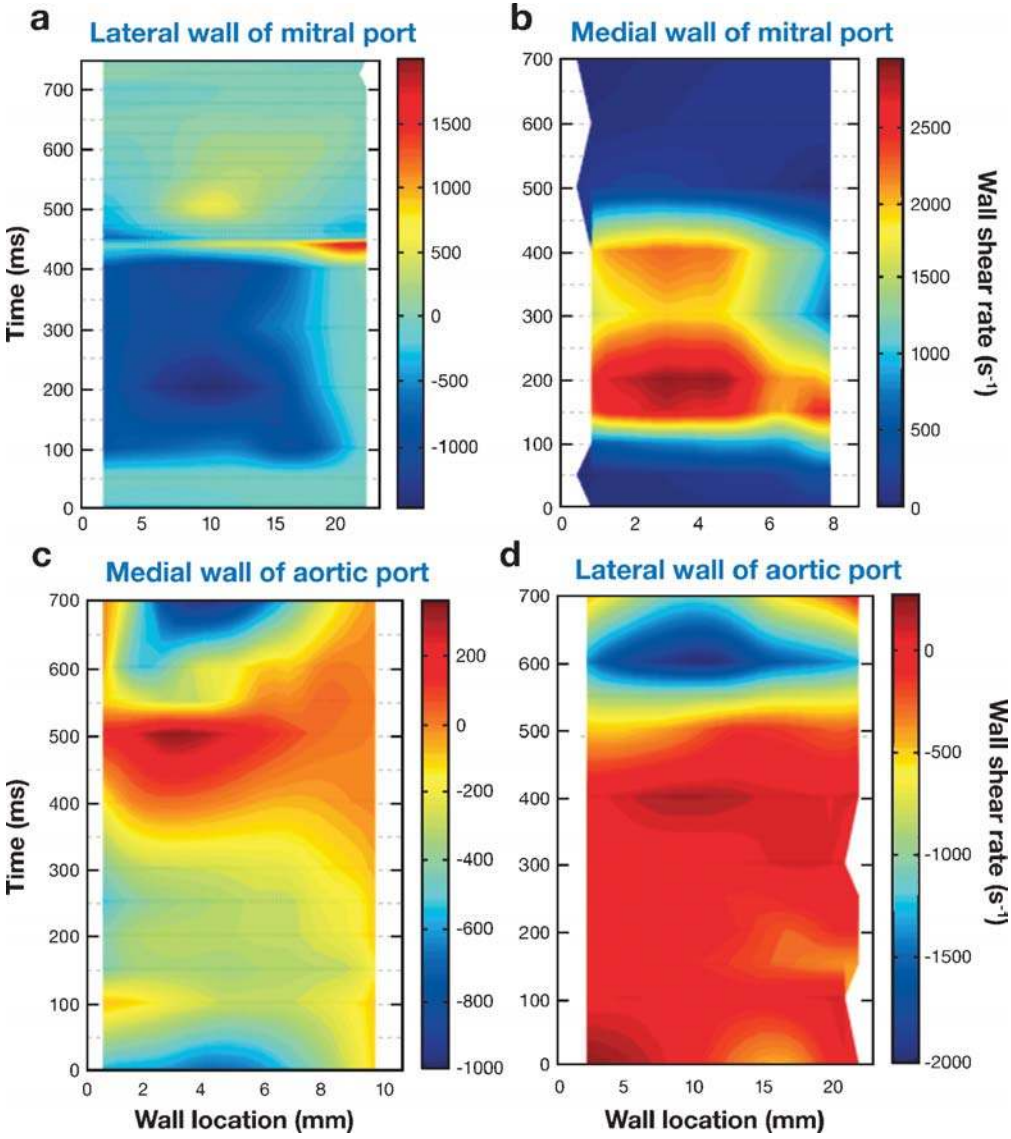

Figure 8

The inlet port's average wall shear rate in time series in the beat cycle from the lateral wall (*a* and *d*) and the medial wall (*b* and *c*) of the mitral port. The lateral wall is the right wall in Figure 7. The wall location axis in a and d corresponds to the vertical axis in Figure 7, where the fully open valve tip position is at the wall location approximately 16 mm. The wall shear rate data in b and c were obtained from magnified particle image velocimetry vector maps of the minor orifice jet region. As a result, the wall location axis in b and c does not coincide directly with the vertical axis shown in Figure 7. The positive direction of the wall location axis in b and c is reversed from that in a and d, where 0 mm corresponds to roughly 23 mm on the vertical axis in Figure 7.

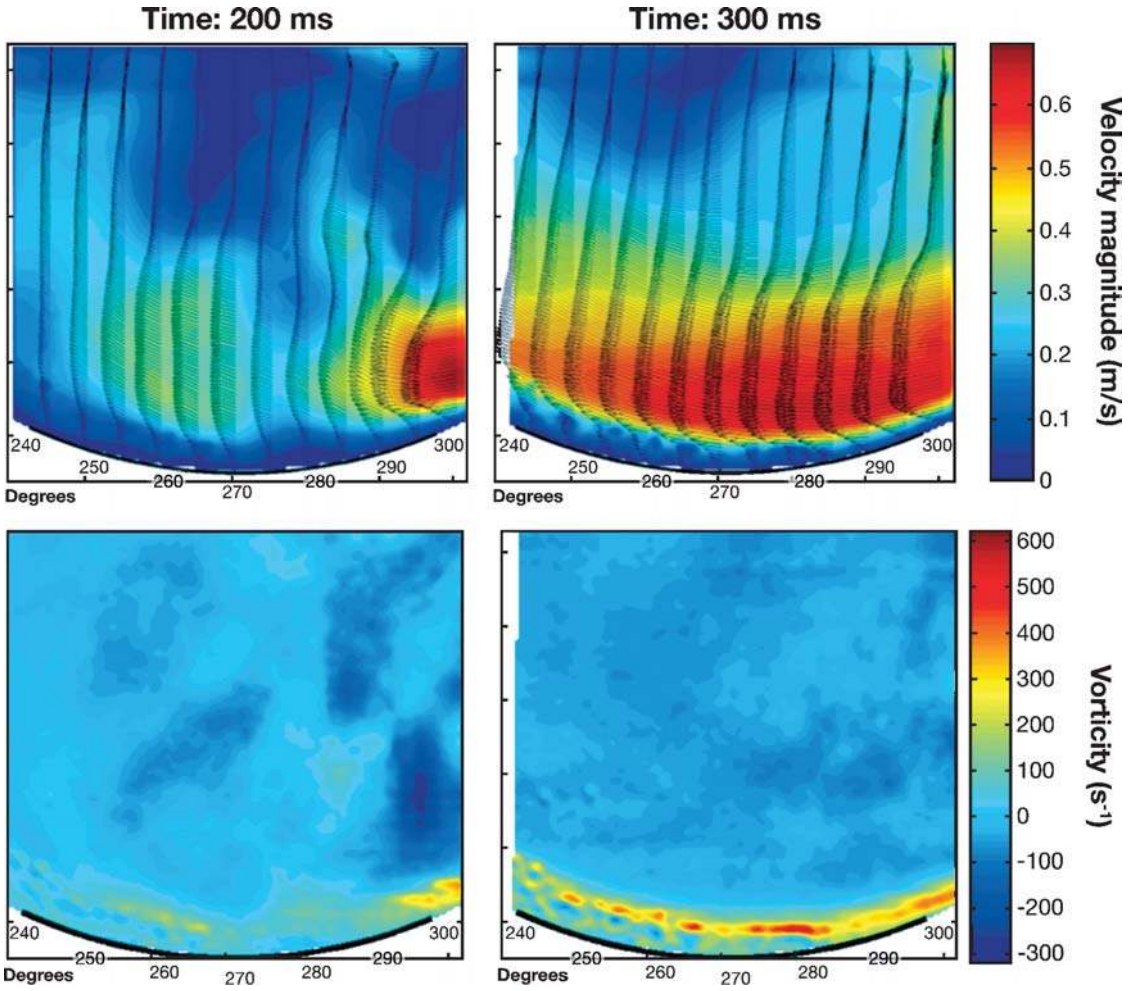

Figure 9

The velocity and vorticity maps of the bottom wall from time 200 ms and 300 ms for the 50-cc Penn State ventricular assist device. This region shows potential for flow separation due to the low velocities measured using particle image velocimetry. (Note: The size of the area is 30 × 30 mm.) (Permission granted from ASME, Hochareon et al. 2004.)

3000 s^{-1}. The secondary inflow jet through the minor orifice of the mitral port had not been previously studied.

The local flow and vorticity fields near the bottom of the device are shown in **Figure 9**. Shear rates for this region are 0–250 s^{-1}. The authors note such low shear rates over the entire cycle are of concern. Similar shear rates are observed at the upper wall region between the valve ports. A rough summary of shear rates in the device is reproduced in **Figure 10**. In general, the wall shear rates observed in the 50-cc device are much lower than those observed by Baldwin et al. (1988) in a 100-cc ventricle.

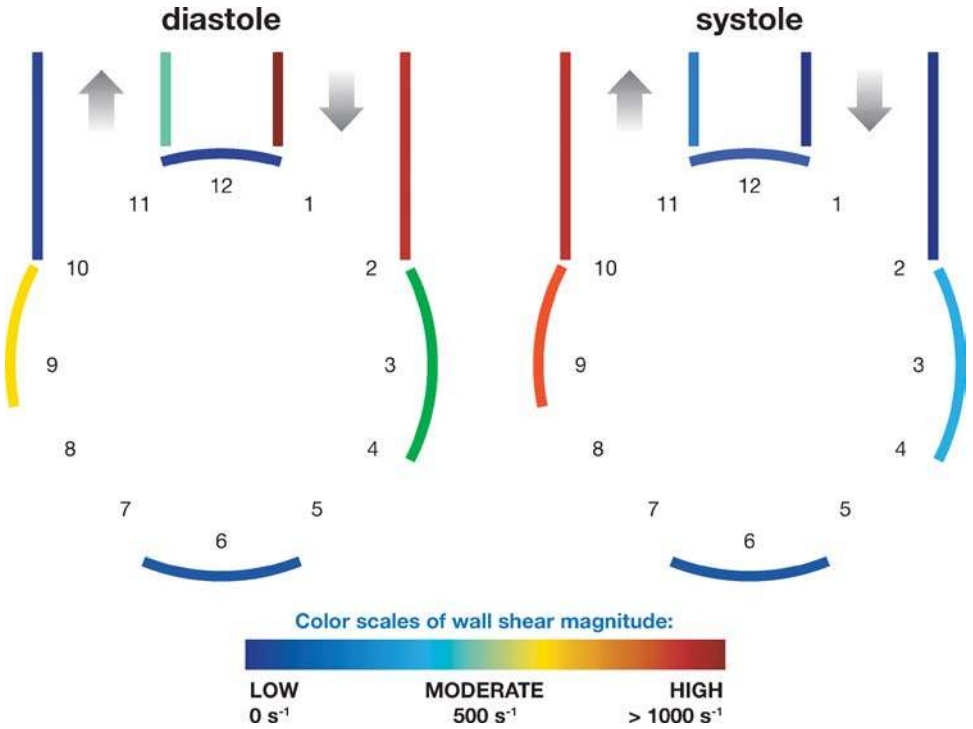

Figure 10

Qualitative summary of wall shear rates within the 50-cc Penn State ventricular assist device during diastole and systole. (Permission granted from ASME, Hochareon et al. 2004.)

Hochareon et al. (2004b) developed refined methods to estimate the wall shear stress from PIV measurements in the artificial ventricle. Issues include the improvement of wall location estimates and the position of the velocity vector in the irregular measurement volumes nearest the wall. The influence of the size of the interrogation region was studied by simulations. Hochareon et al. (2004c) used the refined method for determining wall shear rate to obtain more extensive data in the bottom region of the 50-cc device. Yamanaka et al. (2003) are performing an in vivo study of clot deposition in the 50-cc heart implanted in calves, which shows good correlation with regions of persistent low wall shear. Much more work correlating wall shear and clot formation is warranted.

Oley et al. (2005) recently completed a PIV study of the effect of beat rate and systolic duration on the global flow characteristics in the same 50-cc device. Shorter diastolic times produced a stronger inlet jet and an earlier and stronger diastolic rotation. However, the stronger the diastolic rotation, the larger the separated flow region on the inlet side of the aortic valve. The authors note that the relatively rapid acquisition of whole-flow field data, using PIV, may permit experiments to play a more active role in the design process for artificial devices.

CONCLUSIONS AND FUTURE DIRECTIONS

For artificial ventricles suitable for large adults (>/= 70 cc), clot formation within the ventricle is not generally observed. The major problems are associated with the valves, both with the high stresses in the regurgitant jets and with the influence of cavitation. Activation of the clotting cycle is likely, although the clots do not adhere to the surface of the pump. Smaller pumps show some thrombus deposition in addition to the valve-related problems. Maintaining the inlet Strouhal number near physiologic values is sensible, but clot deposition has been observed in a 50-cc device with a physiologic Strouhal number of about 4.

Details of the local fluid mechanics, particularly of the wall shear stresses, will be critical to the successful design of the smaller pumps. Oley et al. (2005) note that the relatively rapid acquisition of whole-flow field data using PIV will be useful in this regard, but we note that the motion of the formed blood elements and their interaction with the artificial materials are a parallel part of the problem not yet addressed by experiment. Computation of the flow field and motion of the formed elements would be extremely useful, but the problems facing a successful computation are formidable. The flow and species motion are unsteady with valve-induced turbulence (at modest Reynolds number) through some of the cycle: The fluid is shear thinning and viscoelastic; the flow is driven by a flexible sac. Work in this important area seems likely to continue for a long time.

Finally, a good deal of effort is currently directed toward the development and testing of rotary blood pumps including axial and centrifugal flow assist devices (Reul 2003).

ACKNOWLEDGMENTS

We gratefully acknowledge the support of 30 years of continuous National Institutes of Health funding from NHLBI Grants HL13426, HL20356, HL48652, HL62076, RR15930, HV48191, and HV88105. We also appreciate the dedication and hard work from the faculty, engineers, graduate students, technicians, undergraduate students, and support staff at both the University Park and Hershey campuses of Pennsylvania State University during this research endeavor.

LITERATURE CITED

Affeld A. 1979. The state of the art of the Berlin Total Artificial Heart—technical aspects. In *Assisted Circulation*, ed. F Unger, pp. 307–33. New York: Springer Verlag. 653 pp.

Bachmann C, Hugo G, Rosenberg G, Deutsch S, Fontaine AA, et al. 2000. Fluid dynamics of a pediatric ventricular assist device. [Erratum *Artif. Organs* 2000 24:989] *Artif. Organs* 24:362–72

Bachmann C, Kini V, Deutsch S, Fontaine AA, Tarbell JM. 2001. Mechanisms of cavitation and the formation of stable bubbles on the Bjork-Shiley monostrut prosthetic heart valve. *J. Heart Valve Dis.* 11:105–13

Baldwin JT, Tarbell JM, Deutsch S, Geselowitz DB, Rosenberg G. 1988. Hot-film wall shear probe measurements inside a ventricular assist device. *J. Biomech. Eng.* 110:326–33

Baldwin JT, Tarbell JM, Deutsch S, Geselowitz DB. 1989. Mean flow velocity patterns within a ventricular assist device. *ASAIO Trans.* 35:429–33

Baldwin JT, Deutsch S, Geselowitz DB, Tarbell JM. 1994. LDA measurements of mean velocity and Reynolds stress fields within an artificial heart ventricle. *J. Biomech. Eng.* 116:190–200

Baldwin JT, Deutsch S, Geselowitz DB, Tarbell JM. 1990. Estimation of Reynolds stresses within the Penn State left ventricular assist device. *ASAIO Trans.* 36:M274–78

Baldwin JT, Deutsch S, Petrie HL, Tarbell JM. 1993. Determination of principal Reynolds stresses in pulsatile flows after elliptical filtering of discrete velocity measurements. *J. Biomech. Eng.* 115:396–403

Baldwin JT, Deutsch S, Geselowitz DB, Tarbell JM. 1994. LDA measurements of mean velocity and Reynolds stress fields within an artificial heart ventricle. *J. Biomech. Eng.* 116:190–200

Biancucci B, Deutsch S, Geselowitz DB, Tarbell JM. 1999. In vitro studies of gas bubble formation by mechanical heart valves. *J. Heart Valve Dis.* 8:186–96

Brookshier KA, Tarbell JM. 1993. Evaluation of a transparent blood analog fluid: aqueous Xanthan gum/glycerin. *Biorheology* 30:107–16

Chandran KB, Aluri S. 1997. Mechanical valve closing dynamics: relationship between velocity of closing, pressure transients, and cavitation initiation. *Ann. Biomed. Eng.* 25:926–38

Cokelet GR. 1987. The rheology and tube flow of blood. In *Handbook of Bioengineering*, ed. R Skalak, S Chien, 14.1–14.17. New York: McGraw Hill. 932 pp.

Cooley DA. 1969. First human implantation of cardiac prosthesis for staged total replacement of the heart. *ASAIO Trans.* 15:252

Dauzat M, Deklunder G, Aldis A, Rabinovitch M, Burte F, et al. 1994. Gas bubble emboli detected by transcranial Doppler sonography in patients with prosthetic heart valves: a preliminary report. *J. Ultrasound Med.* 13:129–35

Daily BB, Pettitt TW, Sutera SP, Pierce WS. 1996. Pierce-Donachy pediatric VAD: progress in development. *Ann. Thorac. Surg.* 61:437–43

Francischelli DE, Tarbell JM, Geselowitz DB. 1991. Local blood residence times in the Penn State artificial heart. *Artif. Organs* 15:218–24

Gharib M, Rambod E, Shiota T, Sahn D. 1994. Dynamic filling characteristics of the left ventricle of the heart. Presented at *Int. Symp. Biofluid Mech.*, 3rd, Munich, pp. 343–45. Düsseldorf: VDI Verlag

Graf T, Reul H, Detlefs C, Wilmes R, Rau G. 1994. Causes and formation of cavitation in mechanical heart valves. *J. Heart Valve Dis.* 1:S49–64

Hall DP, Moreno JR, Dennis C, Senning A. 1962. An experimental study of prolonged left heart bypass without thoracotomy. *Ann. Surg.* 156:190–96

Hochareon P, Manning KB, Fontaine AA, Deutsch S, Tarbell JM. 2003. Diaphragm motion affects flow patterns in an artificial heart. *Artif. Organs* 27:1102–9

Hochareon P, Manning KB, Fontaine AA, Tarbell JM, Deutsch S. 2004a. Wall shear-rate estimation within the 50cc Penn State artificial heart using particle image velocimetry. *J. Biomech. Eng.* 126:430–37

Hochareon P, Manning KB, Fontaine AA, Tarbell JM, Deutsch S. 2004b. Fluid dynamic analysis of the 50cc Penn State artificial heart under physiological operating conditions using particle image velocimetry. *J. Biomech. Eng.* 126:585–93

Hochareon P, Manning KB, Fontaine AA, Tarbell JM, Deutsch S. 2004c. Correlation of in vivo clot deposition with the flow characteristics in the 50cc Penn State artificial heart: a preliminary study. *ASIAO J.* 50:537–42

Hubbell JA, McIntire LV. 1986. Visualization and analysis of mural thrombogenesis on collagen, polyurethane and nylon. *Biomaterials* 7:354–63

Jarvis P, Tarbell JM, Frangos JA. 1991. An in vitro analysis of an artificial heart. *ASAIO Trans.* 37:27–32

Jin W, Clark C. 1993. Experimental investigation of unsteady-flow behavior within a sac-type ventricular assist device (VAD). *J. Biomech.* 26:697–707

Jin W, Clark C. 1994. Experimental investigation of the pumping diaphragm within a sac-type pneumatically driven ventricular assist device. *J. Biomech.* 27:43–55

Kafesian R, Howanec M, Ward GD, Diep L, Wagstaff LS, Rhee R. 1994. Cavitation damage of pyrolytic carbon in mechanical heart valves. *J. Heart Valve Dis.* 3:52–57

Konertz W, Holger H, Schneider M, Redlin M, Reul H. 1997a. Clinical experience with the MEDOS HIA-VAD system in infants and children: a preliminary report. *Ann. Thorac. Surg.* 63:1138–44

Konertz W, Reul H. 1997b. Mechanical circulatory support in children. *Artif. Organs* 20:657–58

Lamson TC, Rosenberg G, Deutsch S, Geselowitz DB, Stinebring DR, et al. 1993. Relative blood damage in the three phases of a prosthetic heart valve flow cycle. *ASAIO J.* 39:M626–33

LeGallois M, Nancrede NC, Nancrede JG. 1813. *Experiments on the Principle of Life*. Philadelphia: M. Thomas. 328 pp.

Lenker JA. 1978. *Flow studies in artificial hearts and LVAD: an application of flow visualization analysis*. PhD thesis. Pennsylvania State Univ. 198 pp.

Leuer L. 1986. In vitro evaluation of drive parameters and valve selection for the total artificial heart. Presented at *Proc. Int. Symp. Art. Org., Biomed. Eng. and Transpl.*, Salt Lake City, Utah, 47 pp. Salt Lake City: Univ. Utah

Lin HY, Biancucci B, Deutsch S, Fontaine AA, Tarbell JM. 2000. Observation and quantification of gas bubble formation on a mechanical heart valve. *J. Biomech. Eng.* 122:304–9

Mann KA, Deutsch S, Tarbell JM, Geselowitz DB, Rosenberg G, et al. 1987. An experimental study of Newtonian and non-Newtonian Flow dynamics in a ventricular assist device. *J. Biomech. Eng.* 109:139–47

Maymir JC, Deutsch S, Meyer R, Geselowitz DB, Tarbell JM. 1997. Effects of tilting disk valve gap width on regurgitant flow through an artificial heart mitral valve. *Artif. Organs* 21:1014–25

Maymir JC, Deutsch S, Meyer R, Geselowitz DB, Tarbell JM. 1998. Mean velocity and Reynolds stress measurements in the regurgitant jets of tilting disk heart valves in an artificial heart environment. *Ann. Biomed. Eng.* 26:146–56

Mehta SM, Pae WE, Rosenberg G, Snyder AJ, Weiss, WJ, et al. 2001. The LionHeart LVD-2000: a completely implanted left ventricular assist device for chronic circulatory support. *Ann. Thor. Surg.* 71:S156–61

Meyer RS, Deutsch S, Maymir JC, Geselowitz DB, Tarbell JM. 1997. Three-component LDV measurements in the regurgitant flow region of a Björk-Shiley Monostrut mitral valve. *Ann. Biomed. Eng.* 25:1081–91

Meyer RS, Deutsch S, Bachmann CB, Tarbell JM. 2001. Laser Doppler velocimetry and flow visualization studies in the regurgitant leakage flow region of three mechanical heart valves. *Artif. Organs* 25:292–99

Mussivand T, Navarro R, Chen JF. 1988. Flow visualization in an artificial heart using diffuse and planar lighting. *ASAIO Trans.* 34:317–21

National Heart, Lung, and Blood Institute Working Group. 1985. *Guidelines for blood-materials interaction*. NIH Pub. 85-2185. 78. Bethesda, MD: Natl. Heart Lung Blood Inst.

Nevaril C, Hellums J, Alfrey CJ, Lynch E. 1969. Physical effects in red blood cell trauma. *Am. Inst. Chem. Eng. J.* 15:707–11

Oley LA, Manning KB, Fontaine AA, Deutsch S. 2005. Off design considerations of the 50cc Penn State ventricular assist device. *Artif. Organs*. 29:378–86

Park Y, Kim S. 1998. Development and animal study of a pediatric ventricular assist device. *Yonsei Med. J.* 39:154–58

Phillips WM, Brighton JA, Pierce WS. 1972. Artificial heart evaluation using flow visualization techniques. *SAIO Trans* 18:194–99

Phillips WM, Furkay SS, Pierce WS. 1979. Laser Doppler anemometer studies in unsteady ventricular flows. *ASAIO Trans* 25:56–60

Quijano R. 1988. Edwards-Duromedics dysfunctional analysis. Presented at *Proc. Cardiostimulation*, 6th, Monte Carlo

Reul H. 2003. *Overview of rotary blood pump designs*. Presented at Amer. Soc. Artif. Inter. Organs, 49th, Washington, D.C.

Rosenberg G, Phillips WM, Landis D, Pierce WS. 1981. Design and evaluation of The Pennsylvania State University mock circulatory system. *ASAIO J.* 4:41–49

Sallam AM, Hwang NHC. 1984. Human red blood cell hemolysis in a turbulent shear flow: contribution of Reynolds shear stresses. *Biorheology* 21:783–97

Taenaka Y, Takano H, Noda H, Kinoshita M. 1990. A pediatric ventricular assist device: its development and experimental evaluation of hemodynamic effects on postoperative heart failure of congenital heart diseases. *Artif. Organs* 14:49–56

Takano H, Nakatani T. 1996. Ventricular assist systems: experience in Japan with Toyobo pump and Zeon pump. *Ann. Thorac. Surg.* 61:317–22

Tarbell JM, Gunshinan JP, Geselowitz DB, Rosenberg G, Shung KK, et al. 1986. Pulsed ultrasonic Doppler velocity measurements inside a left ventricular assist device. *J. Biomech. Eng.* 108:232–38

Thurston GB. 1996. Viscoelastic properties of blood and blood analogs. In *Advances in Hemodynamics and Hemorheology*, ed. TV How, pp. 1–34. Greenwich, CT: JAI

Walker W. 1974. Cavitation in pulsatile blood pumps. *Adv. Bioeng. New York* pp. 148–50. New York: ASME

Woodward J, Shaffer F, Schaub R, Lund L, Borovetz H. 1992. Optimal management of a ventricular assist device. *ASAIO J.* 38:M216–19

Wootton DM, Ku DN. 1999. Fluid mechanics of vascular systems, diseases, and thrombosis. *Annu. Rev. Biomed. Eng.* 1:299–329

Yamanaka H, Rosenberg G, Weiss WJ, Snyder AJ, Zapata CM, Pae WE. 2003. A multiscale surface evaluation of thrombosis in left entricular assist systems. *ASAIO J.* 49:222

Yoganathan AP, Woo YR, Sung HW. 1986. Turbulent shear stress measurements in the vicinity of aortic heart valve prostheses. *J. Biomech.* 19:422–33

Yoganathan AP, He Z, Casey Jones S. 2004. Fluid mechanics of heart valves. *Annu. Rev. Biomed. Eng.* 6:331–62

Young FR. 1989. *Cavitation*. London: McGraw-Hill

Zapanta CM, Stinebring DR, Sneckenberger DS, Deutsch S, Geselowitz DB, et al. 1996. In vivo observation of cavitation on prosthetic heart valves. *ASAIO J.* 42:M550–55

Annual Review of
Fluid Mechanics

Volume 38, 2006

Contents